Hindawi
Journal of Electrical and Computer Engineering
Volume 2019, Article ID 3605604, 11 pages
https://doi.org/10.1155/2019/3605604

Research Article

Three-Level DC-DC Controlled-Source Circuit of Marine Electromagnetic Detection Transmitter

Haijun Tao, Guopeng Zhang, and Zheng Zheng

Henan Polytechnic University, Jiaozuo, Henan Province 454003, China

Correspondence should be addressed to Guopeng Zhang; zhangguopeng@hpu.edu.cn

Received 7 December 2018; Revised 20 April 2019; Accepted 13 May 2019; Published 13 June 2019

Academic Editor: Herve Morel

Nowadays, marine electromagnetic method is a geophysical method which can effectively explore natural gas hydrate (NGH) resources. This method acquires seafloor structure and distribution laws of mineral resources by transmitting high-power electromagnetic waves to the seafloor, and its detection depth relies on the intensity of transmitted electromagnetic waves. At present, marine electromagnetic transmitter is not proper for transmission of high-power electromagnetic waves, and therefore, a novel controlled-source circuit of soft switching three-level marine electromagnetic transmitter is proposed in this paper, one step-down winding is added at the secondary side of high-frequency transformer in series connection with a linear inductor, asymmetric phase-shift PWM control is used, and soft switching of controlled-source circuit within the overall power range is realized. A detailed analysis of the operation process and circuit characteristics is given, and finally, a prototype is designed. Experimental results indicate that this circuit is of wide ZVS range and high efficiency, and it meets requirements for deep-sea detection of high-voltage power supply transmitter.

1. Introduction

During the exploratory development process of marine resources, due to high drilling cost and high investment risk, global major oil companies will carry out comprehensive prospecting work through multiple marine geophysical methods like an earthquake, gravity, and magnetic force before offshore drilling in order to reduce drilling risks of deepwater oil and gas resources [1]. The operation principle of marine controlled-source electromagnetic detection (MCSEM) is that electromagnetic transmitter is towed to offshore bottom and transmits high-power electromagnetic waves through transmitting dipole, field source signals are collected back by electromagnetic receiving equipment, and through signal processing and inversion, electro-conductive structural features of media below seafloor can be analyzed; it is one of the methods which can effectively explore natural gas hydrate (NGH) resources [2]. Due to attenuation of electromagnetic waves by seawater, the greater the current signals transmitted by the electromagnetic transmitter, the greater the detectable depth, and elevation of transmitting power will bring about problems of heat dissipation and energy loss in seafloor electromagnetic transmission system [3]. It is necessary to reduce internal resistance, reduce internal loss, and improve transmitting efficiency of the transmitter, and research and development of high-efficiency and large-current electromagnetic transmitter system are of great significance to deep-sea detection.

The power supply of marine electromagnetic detection transmitter is a diesel generator which transmits electric energy to the underwater towed vehicle through kilometers of submarine cable transmission, and transmission voltage must be elevated in order to reduce the loss on transmission cable and match load impedance [4]. At present, high-power marine electromagnetic transmitter mainly adopts power frequency transformers + uncontrolled rectification or phase-controlled rectification modes with large volume, poor dynamic characteristic, and restricted transmission power [5]. The literature [6, 7] proposes using diode rectification + PWM full-bridge converter mode, which improves density and dynamic characteristic of transmitter power, but as transmitting power increases, rated voltage

and rated current of switching devices also increase, which reduces switching frequency, enlarges transformer and filter volumes, and degrades power conversion efficiency. Multilevel technology can reduce voltage stress of switching devices; the study in [8] introduces cascading multilevel technology, but there exists a capacitor voltage balance problem. Pinheiro puts forward zero-voltage half-bridge three-level (HB-TL) converter, which reduces voltage stress of switching the device into half of the input voltage [9], and study [10] introduces half-bridge voltage balance control, but it is not appropriate for the high-power situation. Studies [11, 12] introduce hybrid-type full-bridge three-level converters, which reduces input and output current ripples and expands ZVS range of switching devices, as this circuit includes three-level bridge arm and two-level bridge arm, and voltage stress of switching device with two-level bridge arm is input voltage, it is inapplicable to high-voltage input. Literature [13, 14] propose a full-bridge three-level (FB-TL) converter which consists of 8 switching devices, voltage stress of each switching device is half of the input voltage, but the lagging leg is of difficult current commutation and low efficiency. An improved full-bridge three-level converter is introduced and applied to the controlled-source circuit of high-power marine electromagnetic detection transmitter. High-frequency transformer has three secondary windings, where two step-down windings do rectification in parallel so that output current is elevated, another step-down winding is connected to commutation inductor, and this solves difficult current commutation problems of lagging leg under no-load or light-load conditions, realizes soft switching of controlled-source circuit within overall power range, and reduces volumes of input and output filters.

2. Operation Principle of Marine Electromagnetic Detection Transmitter

Marine controlled-source electromagnetic detection system mainly consists of two parts—transmitter and receiver, the former includes diesel generator, three-phase to single-phase power supplies as well as underwater electromagnetic transmitter, and dipolar dragging system, while the latter is a seafloor electromagnetic signal receiving station as shown in Figure 1. The specific operation process is firstly electromagnetic acquisition station is placed according to preset coordinate points, the automatic recording is started, and then the ship will drag underwater electromagnetic transmitter to do the movement at a uniform speed of 3~5 knots according to preset track. Dipole connected to an electromagnetic transmitter will continuously excite electromagnetic waves with different frequencies, and the ship will make a circulation according to the track in order to improve the signal-to-noise ratio of acquired data. Signals will be sent to electromagnetic signal acquisition station which will then automatically release counterweight and emerge from the water after completion of data acquisition. Exploration of the next array or survey line will be implemented.

Marine electromagnetic transmitter, a key component of marine controlled-source electromagnetic exploration system, is responsible for transmitting high-power electromagnetic waves to the seafloor, and it is mainly divided into two parts, namely, shipboard part and underwater part.

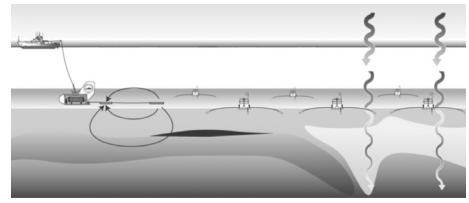

Figure 1: Schematic diagram of operation method of marine controlled-source electromagnetic exploration.

2.1. Shipboard Part. As shown in Figure 2, diesel generator supplies power, and inversion is implemented to obtain single-phase sine alternating current after three-phase rectification and filtering and provide high-voltage single-phase alternating current for underwater tow after the boost transformer T2.

2.2. Underwater Part. Underwater part mainly consists of the controlled-source circuit, transmitting bridge, and transmitting dipole, where the controlled-source circuit is responsible for the transformation of electric energy, namely, transforming single-phase alternating current input by tow into controlled direct current, and transmitting bridge generates time-domain or frequency-domain electromagnetic wave which will be excited by transmitting dipole to the seafloor. At present, the controlled-source circuit of marine electromagnetic transmitter is diode uncontrolled or thyristor phase-controlled rectification type as shown in Figure 3.

Shipboard single-phase power supply is transmitted to underwater tow through photoelectric composite cable, single-phase alternating current is regulated by the power frequency step-down transformer inside the tow, diode uncontrolled rectification or thyristor phase-controlled rectification and filtering are used to obtain low-voltage direct current, and then frequency-controllable square wave alternating current will be generated through inversion of transmitting bridge and excited to the seafloor through transmitting dipole. Diode uncontrolled rectification technology is quite simple and has been widely applied in the high-power transmitter. As uncontrolled rectification circuit cannot regulate voltage amplitude, it usually controls the output voltage through generator excitation, but excitation regulation will influence the revolving speed of the generator, which results in large voltage fluctuation. Consequently, dynamic response of regulation is slow, and thyristors can replace power diodes to constitute phase-controlled rectifier bridge which can control voltage amplitude, but it will cause reduction of power factor.

Therefore, the PWM converter is proposed to replace uncontrolled or phase-controlled rectifier as shown in Figure 4. Single-phase alternating current is inverted into high-frequency alternating current after diode rectification

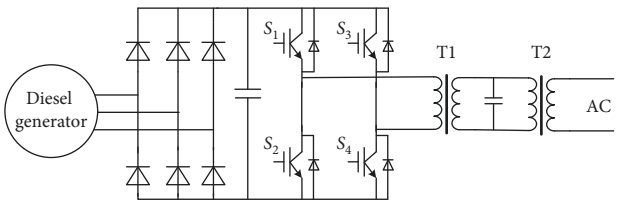

Figure 2: Shipboard power supply circuit of marine transmitter.

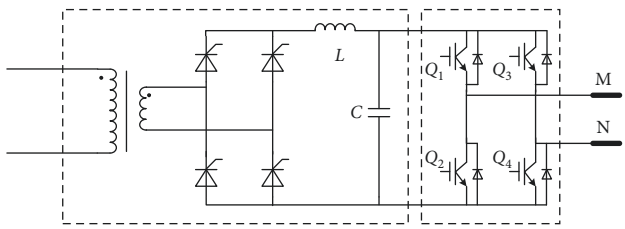

Figure 3: Controlled-source transmitter circuit using phase-controlled rectification.

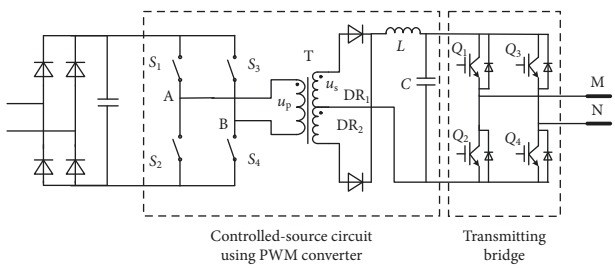

Figure 4: Transmitter circuit using PWM converter.

through the high-frequency isolation step-down transformer, it is rectified into low-voltage direct current, and then a kind of time-domain or frequency-domain electromagnetic waves are output through the transmitting bridge. When input voltage or load current goes through disturbance, the circuit output will be influenced, so it is necessary to design a closed-loop control system to regulate the width of output square wave impulse voltage of inverter bridge in order to maintain output stability so as to control the output voltage.

Compared with the controlled-source circuit of uncontrolled or phase-controlled rectification mode, PWM transformation mode seems quite complicated but with unique advantages: (1) functions of the high-frequency transformer are mainly wide-range voltage regulation realized separately, its operating frequency is tens of kHz or even higher, and transformer volume is greatly reduced; (2) high control precision: control cycle of the phase-controlled rectification-type circuit is half of single-phase AC cycle, while control cycle of PWM transformation-type circuit is a switching cycle, so the difference between the two reaches dozens of times, and the control performance of PWM transformation-type circuit is obviously improved; (3) as operation frequency is high, filter volume is also greatly reduced so that the power density of the transmitter is improved.

High-power PWM transformer is generally full-bridge (ZVS-FB) PWM converter, and in this case, the capacity of switching device must be increased in order to improve transmitting power, which will then cause reduction of switching frequency, enlargement of transformer and filter volumes, and reduction of transformation efficiency of electric energy, so it cannot meet deep marine exploration requirements. Then a full-bridge three-level (TL) DC/DC controlled-source circuit will be introduced and switching device bears 1/2 of input voltage, and meanwhile, switching device can realize soft switching within the whole power range to reduce switching loss and improve circuit efficiency. The circuit can meet the requirements of high-power electromagnetic wave transmission with input voltage 1500 V and output current 500 A.

3. Three-Level Controlled-Source Circuit

3.1. Circuit Topology. A full-bridge three-level (FB-TL) converter is introduced as shown in Figure 5 in reference [15], where switching devices $S_1 \sim S_4$ (including $D_1 \sim D_4$ and $C_{s1} \sim C_{s4}$), clamping diodes D_9 and D_{10}, and flying capacitor C_{ss1} constitute left-side bridge arm, switching devices $S_5 \sim S_8$ (including $D_5 \sim D_8$ and $C_{s5} \sim C_{s8}$), clamping diodes D_{11} and D_{12}, and flying capacitor C_{ss2} constitute right-side bridge arm and two bridge arms jointly input voltage-divider capacitors C_{d1} and C_{d2}, L_s is the resonant inductor, n is the turn ratio of transformer primary winding to rectification winding. The circuit is suitable for high-voltage and high-power applications since each switch is subjected to half of the input voltage.

However, the circuit with multiple lagging legs is difficult to commutate. If the resonant inductance L_s is increased directly, serious duty cycle loss and circulating current loss will occur. Therefore, an improved full-bridge three-level circuit is proposed as a DC/DC controllable source circuit as shown in Figure 6. It has two step-down windings rectifiers in parallel, and one step-down winding was added at the secondary side of the high-frequency transformer in series connection with a linear inductor L_c, and L_r is the leakage inductor of the high-frequency transformer. The former is used to increase the output current; the latter is used to ensure the devices soft switching in full power scope. The auxiliary inductor L_c at a secondary winding can reduce the loss on commutation inductor due to the low voltage and current at a secondary winding and reduce the influence of duty cycle loss.

3.2. Analysis of the Operation Process. During the operation process analysis, it is assumed that

(1) All power diodes, switching devices, inductors, and capacitors are ideal devices

(2) $C_{s1} = C_{s4} = C_{chop}$,
$C_{s2} = C_{s3} = C_{s5} = C_{s6} = C_{s7} = C_{s8} = C_{lag}$,
$C_{ss1} = C_{ss2} = C_{ss}$, $C_{ss} \gg C_{chop}$, $C_{ss} \gg C_{lag}$

(3) $L \gg L_r/n^2$, where L is filter inductance, and it is large enough and can be regarded as a constant current source

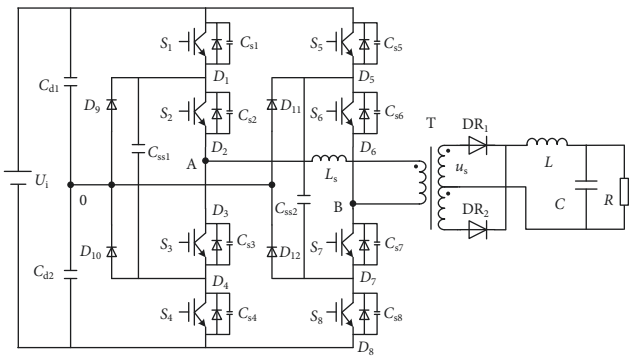

Figure 5: The conventional full-bridge three-level circuit.

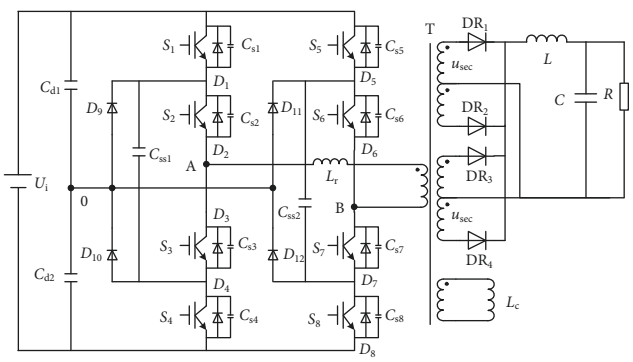

Figure 6: The improved three-level controlled-source circuit.

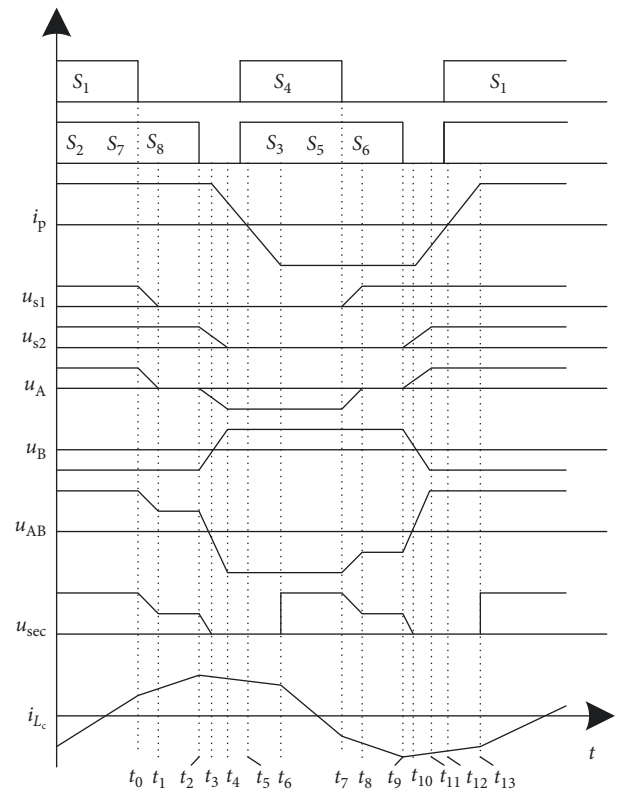

Figure 7: Operation waveforms of three-level controlled-source circuit.

(4) Parameters of two rectifying-circuit devices at the secondary side of the transformer are consistent under the same operation mode, and the only single rectifying circuit is taken into consideration in the analysis

Three conditions should be met by the optimal control mode: (1) power transmission is the maximum under the same duty ratio; (2) filtering inductive current pulsation is the minimum; and (3) switching devices realize soft switching [15] under asymmetric phase-shift PWM control mode, and main operation waveforms are as shown in Figure 7. Turn-on times of S_1 and S_2, S_7, and S_8 (or S_4 and S_3, S_5, and S_6) are the same but with different turn-off times. PWM (pulse width modulation) is used for drive signals of S_1 S_4, while signals driven by lagging leg maintain maximum pulse width. The output voltage is controlled by modulating pulse widths of drive signals S_1 and S_4. S_1 and S_4 are called leading legs, and other switching devices are lagging legs. This control mode is easy for the realization of digitalization, which overcomes problems like control precision and poor flexibility of dedicated chips for traditional phase-shift control. This circuit totally has 14 operation modes.

Mode 0. t_{0-} (Figure 8).

At t_{0-}, switching devices S_1, S_2, S_7, and S_8 are turned on, the primary current of the transformer is $i_p = I_0/n$, the voltage at AB points is $u_{AB} = U_i$, rectifying diode DR_1 is turned on, and DR_1 is turned off. The voltage at two ends of

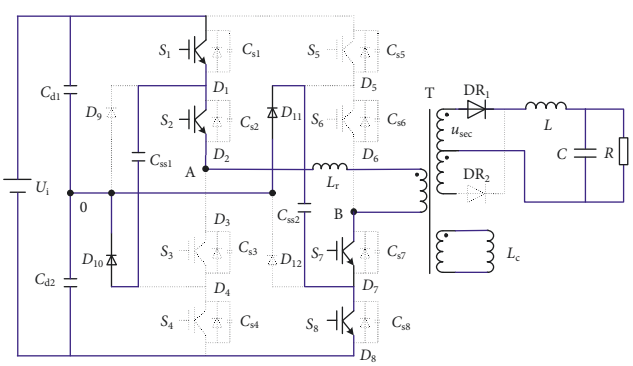

Figure 8: Equivalent circuit of mode 0.

capacitors C_{d1} and C_{d2} in parallel is $U_i/2$, where C_{d1} charges flying capacitor C_{ss1} through branches S_1, C_{ss1}, and D_{10} and C_{d2} charges flying capacitor C_{ss2} through branches S_8, C_{ss2}, and D_{11} until $U_i/2$. Under the function of flying capacitors, voltage stresses of S_3, S_4, S_5, and S_6 are all $U_i/2$. Commutation inductor current starts being increased in a forward direction from maximum reverse current $I_{L_{c0}}$, and commutation inductor current is as follows:

$$i_{L_c}(t) = -I_{L_{c0}} + \frac{1}{L_c}\int_0^{t_0} \frac{U_i}{m} dt, \tag{1}$$

where m is turn ratio of transformer primary winding to commutation winding.

As the output filter inductance L is large enough, the output current I_o is approximately constant within one

switching period. Therefore, the primary current i_p of transformer consists of conversion value of commutation inductor current i_{L_c}, conversion value of output current I_o, and transformer leakage-inductance current i_{L_r}, namely,

$$i_p(t) = \frac{I_o}{n} + \frac{i_{L_c}(t)}{m} + i_{L_r}(t). \tag{2}$$

Mode 1. $[t_{0+}, t_1]$ (Figure 9).

At t_0, the switching device S_1 is turned off, and primary current i_p is transferred from S_1 to its shunt capacitor C_{s1} to charge C_{s1}. As the flying capacitor C_{ss1} is in parallel with S_2 and S_3, voltage sum of C_{s1} and C_{s4} is $U_i/2$, and C_{s4} is discharged when C_{s1} is charged. As C_{s1} starts increasing from zero, S_1 is turned off at zero voltage. In this stage, the primary side outputs power to the secondary side, as filter inductance is large enough, the primary current i_p of the transformer basically remains constant, and C_{s1} voltage increases linearly while C_{s4} voltage decreases linearly.

$$\begin{aligned} u_{C_{s1}}(t) &= \frac{I_{p0}}{2C_{lead}}(t - t_0), \\ u_{C_{s4}}(t) &= \frac{U_i}{2} - u_{C_{s1}} = \frac{U_i}{2} - \frac{I_{p0}}{2C_{lead}}(t - t_0). \end{aligned} \tag{3}$$

Till t_1, the voltage of C_{s4} declines to zero and the voltage of C_{s1} is charged to $U_i/2$. In this case, the commutation inductor current is

$$i_{L_c}(t) = i_{L_c}(t_0) + \frac{1}{L_c}\int_{t_0}^{t_1} \frac{(U_i/2) + u_{C_{s4}}}{m} dt. \tag{4}$$

Mode 2. $[t_1, t_2]$ (Figure 10).

At t_1, as C_{s4} voltage reduces to zero, D_4 is naturally turned on. If the voltage of the flying capacitor C_{ss1} is slightly reduced, then D_9 is turned on, and C_{s4} provides energy for the load. In this stage, under the function of flying capacitors, C_{s4} voltage maintains zero, so S_4 can be turned on at any time before t_5 at zero voltage, which indicates that asymmetric phase-shift PWM control is feasible. In this case, the voltage at AB points is $U_i/2$, and commutation inductor current is

$$i_{L_c}(t) = i_{L_c}(t_1) + \frac{1}{L_c}\int_{t_1}^{t_2} \frac{U_i}{2m} dt. \tag{5}$$

Mode 3. $[t_2, t_3]$ (Figure 11).

At t_2, S_2, S_7, and S_8 are turned off. At left-side bridge arm, i_p is transferred from S_2 to charge C_{s2}. Under the function of flying capacitors, C_{s3} will certainly be discharged while C_{s2} is charged, and S_2 is turned off at zero voltage. At right-side bridge arm, i_p is transferred from S_7 and S_8 to C_{s5}, C_{s6}, C_{s7}, and C_{s8} to charge C_{s7} and C_{s8} to discharge C_{s5} and C_{s6}, and S_7 S_8 are turned off at zero voltage. Up to t_3, u_{AB} declines to zero. In this stage, the primary side still outputs power to the secondary side, the primary current i_p is basically constant, so both charging and discharging processes of capacitors are linear.

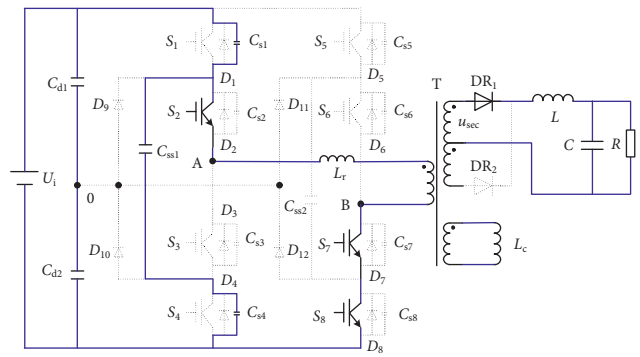

Figure 9: Equivalent circuit of mode 1.

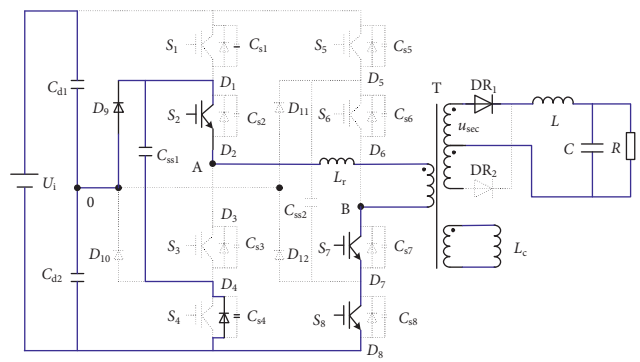

Figure 10: Equivalent circuit of mode 2.

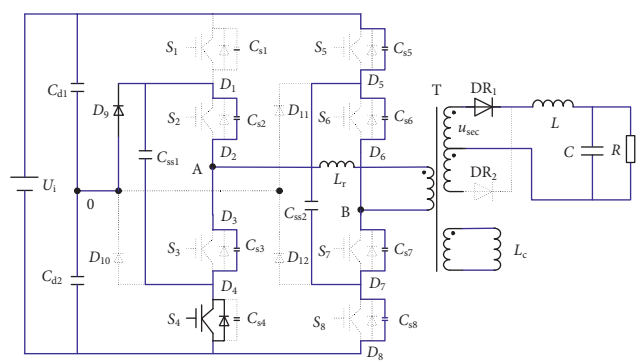

Figure 11: Equivalent circuit of mode 3.

$$\begin{aligned} u_{C_{s2}}(t) &= \frac{I_{p0}}{2C_{lag}} * (t - t_2), \\ u_{C_{s3}}(t) &= \frac{U_i}{2} - u_{C_{s2}}(t) = \frac{U_i}{2} - \frac{I_{p0}}{2C_{lag}} * (t - t_2), \\ u_{C_{s7}}(t) &= u_{C_{s8}}(t) = \frac{I_{p0}}{2C_{lag}} * (t - t_2), \\ u_{C_{s5}}(t) &= u_{C_{s6}}(t) = \frac{U_i}{2} - \frac{I_{p0}}{2C_{lag}} * (t - t_2). \end{aligned} \tag{6}$$

At the time, converting inductor current is

$$i_{L_c}(t) = i_{L_c}(t_2) + \frac{1}{L_c}\int_{t_2}^{t_3} \frac{(U_i/2) - u_{C_{s2}}}{m} dt. \quad (7)$$

Up to t_3, u_{AB} declines to zero, and commutation inductor current reaches peak value $I_{L_{c0}}$. Here, $u_{C_{s3}} = U_i/3$, $u_{C_{s2}} = U_i/6$, $u_{C_{s7}} = u_{C_{s8}} = U_i/6$, and $u_{C_{s5}} = u_{C_{s6}} = U_i/3$.

Mode 4. $[t_3, t_4]$ (Figure 12).

At t_3, u_{AB} declines to zero, so does secondary winding voltage, and rectifying diodes are all turned on. As at the time commutation inductor current reaches peak value, commutation inductor current charges C_{s2}, C_{s7}, and C_{s8} discharges C_{s3}, C_{s5}, and C_{s6} until t_4 when voltages of C_{s3}, C_{s5}, and C_{s6} are reduced to zero. Commutation inductor and a number of windings are reasonably designed, so soft switching of S_2, S_7, and S_8 can be easily realized, and then

$$\begin{aligned}
i_p(t) &= I_{p0}\cos\omega_1(t-t_3),\\
u_{C_{s2}}(t) &= \frac{U_i}{6} + \frac{I_{p0}}{2} * \sqrt{\frac{2(L_r+L_c)}{3C_{lag}}}\sin\omega_1(t-t_3),\\
u_{C_{s3}}(t) &= \frac{U_i}{3} - \frac{I_{p0}}{2} * \sqrt{\frac{2(L_r+L_c)}{3C_{lag}}}\sin\omega_1(t-t_3),\\
u_{C_{s7}}(t) &= u_{C_{s8}}(t) \qquad (8)\\
&= \frac{U_i}{6} + \frac{I_{p0}}{2} * \sqrt{\frac{2(L_r+L_c)}{3C_{lag}}}\sin\omega_1(t-t_3),\\
u_{C_{s5}}(t) &= u_{C_{s6}}(t)\\
&= \frac{U_i}{3} - \frac{I_{p0}}{2} * \sqrt{\frac{2(L_r+L_c)}{3C_{lag}}}\sin\omega_1(t-t_3),
\end{aligned}$$

where $\omega_1 = (1/\sqrt{2(L_r+L_c)C_{lag}/2})$.

At t_4, the value i_p is

$$I_p(t_4) = \sqrt{I_{p0}^2 - \frac{2C_{lag}}{3(L_r+L_c)}U_i^2}. \quad (9)$$

Mode 5. $[t_4, t_5]$ (Figure 13).

At t_4, currents of commutation inductor do not decline to zero yet; D_3, D_5, and D_6 are naturally turned on, current i_p continues to reduce, and up to t_5, it presents linear decline to zero, so S_3, S_4, S_5, and S_6 can be turned on at zero voltage at any time in this stage. Current i_p is

$$i_p = I_p(t_4) - \frac{U_i}{L_r}(t-t_4) - \frac{U_i}{mL_c}(t-t_4). \quad (10)$$

Mode 6. $[t_5, t_6]$ (Figure 14).

At t_5, S_3, S_4, S_5, and S_6 are turned on, and i_p starts being increased in the inverse direction. In this case, i_p does not reach a primary converted value of load current I_{p0}, two rectifying diodes are still simultaneously turned on, i_p and increases in the inverse direction. Up to t_6, the absolute value of i_p increases to I_{p0}.

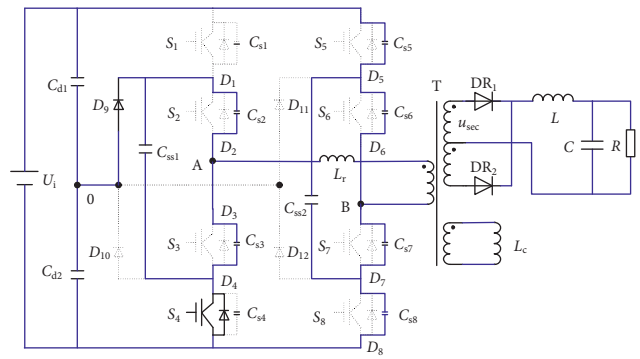

Figure 12: Equivalent circuit of mode 4.

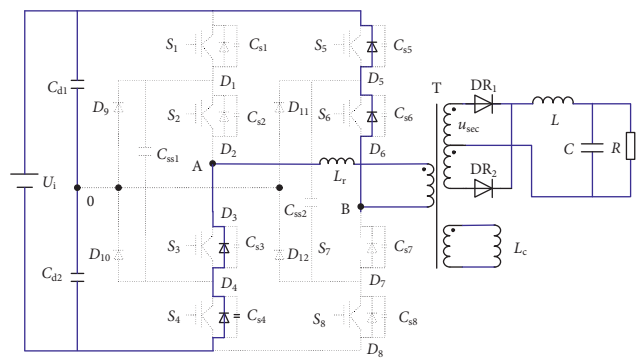

Figure 13: Equivalent circuit of mode 5.

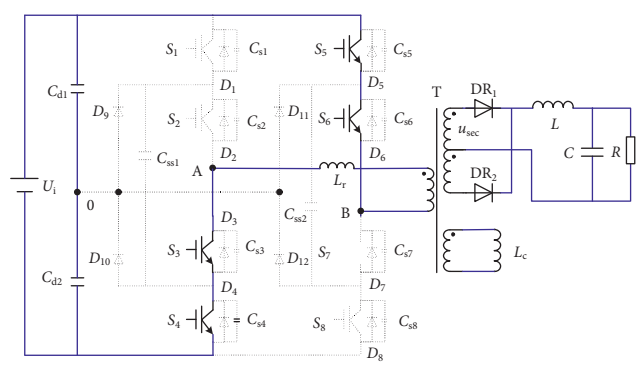

Figure 14: Equivalent circuit of mode 6.

Mode 7. $[t_6, t_7]$ (Figure 15).

At t_6, as i_p reaches I_{p0}, rectifying diode DR_1 is turned off, and the transformer provides energy for the load through DR_2. As during the switching process, energies of C_{ss1} and C_{ss2} are somewhat released, and at the time, there will be a process in which C_{d2} charges C_{ss1} through branches D_9, C_{ss1}, and S_4. C_{d1} charges C_{ss2} through branches D_{12}, C_{ss2}, and S_5. Up to t_7, the circuit starts the operation process of the next half period, which will not be described in details.

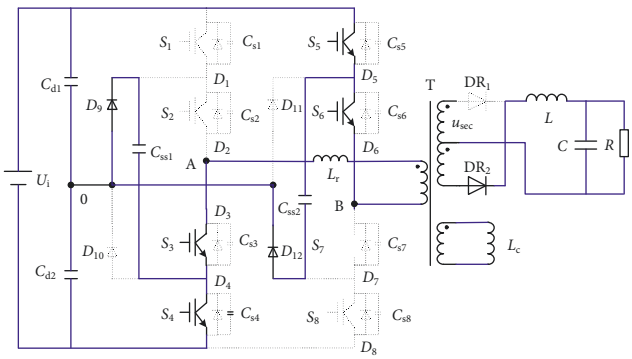

Figure 15: Equivalent circuit of mode 7.

4. Circuit Characteristics

4.1. Functions of Flying Capacitors and Flywheel Diodes. The operation process of full-bridge three-level DC/DC controlled-source circuit mentioned above has made a detailed analysis of flying capacitors and flywheel diodes at left-side bridge arm. Now functions of flying capacitors and flywheel diodes at right bridge arm will analyze. It can be known from driving waveforms in Figure 7 that switching devices S_5 and S_6 (or S_7 and S_8) of right three-level bridge arm are simultaneously turned on and turned off; however, in the actual circuit, differences will certainly exist in turning on and turning off of S_5 and S_6 (or S_7,S_8). If there are no flying capacitors or flywheel diodes, it will possibly cause nonuniform voltage stress of switching devices. When switching device is turned on at ZVS, its antiparallel diodes have been turned on, and at the time, differences existing in turning on of switching devices will not cause nonuniformity of voltage stress of switching devices. Functions of flying capacitors and flywheel diodes will be mainly discussed under differences of turning off of switching devices.

It is assumed that switching devices S_5 and S_6 are simultaneously turned on and turned off; switching devices S_7 and S_8 will be simultaneously turned on but they cannot be simultaneously turned off. The discussion will be made under two circumstances: S_7 is turned off before and after S_8.

4.1.1. Switching Device S_7 Is Turned Off before S_8. Figure 16 gives main waveforms when switching device S_7 is turned off before S_8. Before t_0, switching devices S_1, S_2, S_7, and S_8 are turned on. At t_0, switching devices S_7 and S_8 should be simultaneously turned off at first; the switching device S_7 is turned off while S_8 is still under on state due to the difference of characteristics of circuit devices. i_p charges capacitor C_{s7} and discharges the capacitor C_{s6} through a flying capacitor C_{ss2} and i_p reduces.

At t_1, S_8 is turned off, and i_p charges the capacitor C_{s8} and discharges the capacitor C_{s5} through the flying capacitor C_{ss2}. Meanwhile, i_p continues to charge the capacitor C_{s7} and discharge C_{s6} through the flying capacitor C_{ss2}.

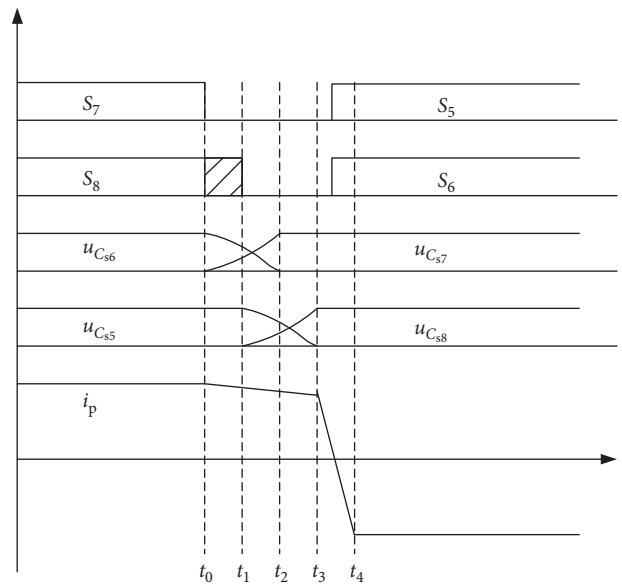

Figure 16: Main waveforms when S_7 is turned off before S_8.

$$i_p = i_{C_{s6}} + i_{C_{s7}}, \tag{11}$$

$$i_{C_{s5}} = i_{C_{s6}} + i_{C_{ss2}}, \tag{12}$$

$$i_{C_{s8}} = i_{C_{s7}} - i_{C_{ss2}}. \tag{13}$$

Through the addition of formula (12) and (13), the following can be obtained by combining (11):

$$i_p = i_{C_{s5}} + i_{C_{s8}} = i_{C_{s6}} + i_{C_{s7}}. \tag{14}$$

It can be known from formula (14) that the current which discharges shunt capacitor of the lagging leg is i_p and energy which realizes ZVS of the lagging leg is provided by commutation inductor.

At t_2, the voltage of the capacitor C_{s6} reduces to zero if the primary current does not reduce to zero yet; the diode D_6 is naturally turned on, and the switching device S_6 can be turned on at zero voltage. i_p continues to charge the capacitor C_{s8} through a flying capacitor C_{ss2} and discharge capacitor C_{s5}. At t_3, the voltage of the capacitor C_{s5} reduces to zero, if the primary current does not reduce to zero yet, the diode D_5 will be naturally turned on, and switching device S_5 can be turned on at zero voltage. As driving signals of S_5 and S_6 are the same, turning-on signals are sent to S_5 and S_6 at t_3, which can be turned on at zero voltage.

4.1.2. Switching Device S_7 Is Turned Off after S_8. Figure 17 gives main waveforms when switching device S_7 is turned off after S_8. Before t_0, the switching device S_8 is turned off while S_7 is still turned on, primary current i_p charges capacitor C_{s7} and discharges the capacitor C_{s5} through a flying capacitor C_{ss2}, and i_p reduces. At t_1, the switching device S_7 is turned off, i_p charges capacitor C_{s7} and discharges the capacitor C_{s6} through the flying capacitor

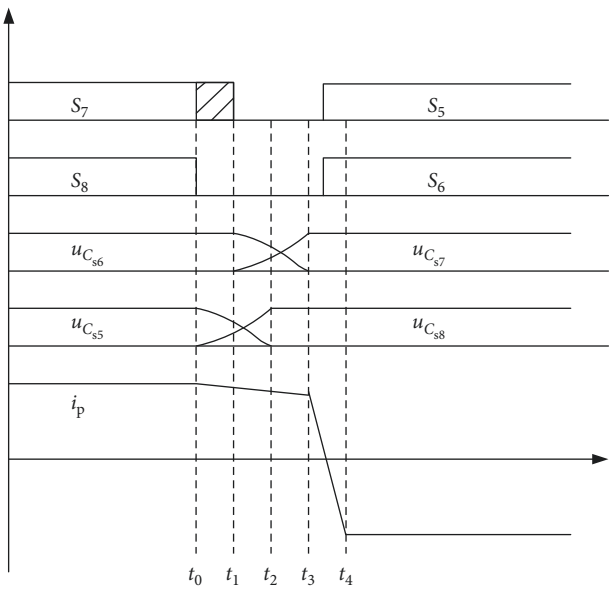

Figure 17: Main waveforms when S_7 is turned off after S_8.

C_{ss2}. Meanwhile, i_p continues to charge C_{s8} and discharge the capacitor C_{s6} through the flying capacitor C_{ss2}. Formula (14) indicates that the current which discharges shunt capacitance of lagging leg is i_p, and the energy which realizes ZVS of the lagging leg is provided by commutation inductor. At t_2, the voltage of the capacitor C_{s5} reduces to zero if the primary current does not decline to zero yet, the diode D_5 is naturally turned on, and the switching device S_5 can be turned on at zero voltage. i_p continues to charge the capacitor C_{s7} through a flying capacitor C_{ss2} and discharge capacitor C_{s7}. At t_3, the voltage of the capacitor C_{s6} reduces to zero, the diode D_6 is naturally turned on, and the switching device S_6 can be turned on at zero voltage.

For right three-level bridge arm, if there is no flying capacitor or flywheel diode, voltage stress of the switching device which is turned off firstly will exceed $U_i/2$ when the above two switching devices or below two switching devices are not simultaneously turned off, which will cause an imbalance of voltage stress borne by switching devices.

The object of flywheel diode is to provide channel supplementing energy for flying capacitor and to make the voltage of the flying capacitor maintain at $U_i/2$. It can be seen from the above analysis that flying capacitor not only realizes decoupling of charging and discharging processes of parallel capacitors of switching devices but also keeps voltage stress of switching devices at $U_i/2$, which avoids an imbalance of voltage stress caused by differences of turning on and turning off of two pairs of switching devices.

4.2. Conditions of Soft Switching

4.2.1. Soft Switching of the Leading Leg. It can be known from the previous analysis that to realize ZVS, the leading leg must have enough energy to take away electric charge on a parallel capacitor C_{s4} of switching device S_4 and discharge parallel capacitor C_{s1} of switching device S_1 which is turned off; then, the energy used by the leading leg to realize ZVS is

$$E_{chop} \geq \frac{1}{2}C_{s1}\left(\frac{U_i}{2}\right)^2 + \frac{1}{2}C_{s4}\left(\frac{U_i}{2}\right)^2 = \frac{1}{4}C_{chop}U_i^2. \quad (15)$$

This energy mainly comes from primary converted value from load current. As output filter inductance is large enough, it is approximately believed that the current converted from constant current source to the primary side will easily let leading leg be turned on at zero voltage.

4.2.2. Soft Switching of Lagging Leg. Three-level DC/DC controlled-source circuit has three lagging devices which are simultaneously turned off. During the turning off process, ZVS of the lagging leg can be realized only by charging parallel capacitors on lagging device which is turned off and by completely discharging parallel capacitors on three lagging devices. Taking turning off of S_2, S_7, and S_8 as an example, they are divided into two stages as shown in Figure 3. In stage I, u_{AB} reduces to zero, and corresponding to mode 3, energy is mainly provided by the current converted from output filter inductor in this stage:

$$\begin{aligned} E_{lag1} &\geq \frac{1}{2}\left(C_{s2}+C_{s7}+C_{s8}\right)\left(\frac{U_{dc}}{3}\right)^2 \\ &\quad + \frac{1}{2}\left(C_{s3}+C_{s5}+C_{s6}\right)\left(\frac{U_{dc}}{6}\right)^2 \\ &= \frac{5}{24}C_{lag}U_{dc}^2. \end{aligned} \quad (16)$$

In Stage II, u_{AB} rises to U_i, and corresponding to mode 4, energy is mainly provided by the current converted from commutation inductor in this stage.

$$\begin{aligned} E_{lag2} &\geq \frac{1}{2}\left(C_{s2}+C_{s7}+C_{s8}\right)\left[\left(\frac{U_{dc}}{2}\right)^2 - \left(\frac{U_{dc}}{6}\right)^2\right] \\ &\quad + \frac{1}{2}\left(C_{s3}+C_{s5}+C_{s6}\right)\left(\frac{U_{dc}}{3}\right)^2 \\ &= \frac{1}{2}C_{lag}U_{dc}^2. \end{aligned} \quad (17)$$

The energy of the commutation inductor must satisfy the following expression:

$$\frac{1}{2}L_c\left(\frac{U_{dc}T_s}{4mL_c}\right)^2 = \frac{1}{2}C_{lag}U_{dc}^2. \quad (18)$$

Then

$$L_c = \frac{T_s^2}{16m^2C_{lag}}. \quad (19)$$

If ZVS is realized when the output current is 1/5 of the designed full load, the duty cycle loss of conventional three-level converter is as follows:

$$L_c' = \frac{25C_{lag}n^2U_{dc}^2}{I_o^2}. \quad (20)$$

4.3. Duty Ratio Loss. Due to the existence of leakage inductance of the transformer, it will certainly bring about

duty ratio loss. It can be known from previous analysis that inverted output voltage u_{AB} has reached $-U_i$ at t_4, and this time is corresponding controlled duty ratio, but voltage u_s of secondary side of transformer does not rise to nU_{dc} until t_6, and this time is corresponding to effective duty ratio, and difference value between the two times is time of duty ratio loss as shown in Figure 3.

$$t_{45} = \frac{I_p(t_4)L_r}{U_i}, \quad t_{56} = \frac{I_{p0}L_r}{U_i}. \tag{21}$$

Duty ratio loss is as follows:

$$D_{loss} = \frac{t_{45} + t_{56}}{T_s} = \frac{2\left(I_p(t_4) + I_{p0}\right)L_r}{T_s U_i}. \tag{22}$$

The duty cycle loss of conventional three-level converter is as follows:

$$D'_{loss} = \frac{2\left(I_p(t_4) + I_{p0}\right)L_s}{T_s U_i}. \tag{23}$$

As commutation inductor is used to provide energy for turning off of lagging leg, leakage inductance should be as small as possible during the transformer design process, and in this way, $L_s \gg L_r$, so duty ratio loss of three-level DC/DC controlled-source circuit after addition of commutation inductor is very small.

4.4. Selection of Flying Capacitor. When load current changes, the stability of a flying capacitor must be ensured. Primary current discharges the parallel capacitor through the flying capacitor during the turning off interval of S_1 and discharges parallel capacitor C_{s1} during the turning off interval of S_4. Under the steady state of the circuit, the flying capacitor is charged to $U_i/2$, and $U_i/2$ can be kept constant only when flying capacitance value is large enough, and capacitance value is related to the current flowing through it and expected voltage ripple, so capacitance value is as follows:

$$C_{ss} \geq \frac{I_{p0}t_d}{\Delta U_{C_{ss}}}, \tag{24}$$

where t_d is the dead time and $\Delta U_{C_{ss}}$ is the expected ripple voltage. In order to solve initial charging balance problem of the flying capacitor, a 470 k/2 W resistor is connected in parallel to it, and meanwhile, a 470 k/2 W resistor is in parallel connection with switching devices S_1 and S_4, which can compensate the initial imbalance of capacitance voltage.

5. Experimental Results

A prototype of a marine electromagnetic detection transmitter is used to verify the effectiveness of the contents stated above. Parameters are as follows: input voltage $U_i = 540$ V, output voltage $U_o = 30$ V, output current $I_o = 200$ A, and switching frequency $f_s = 20$ kHz; commutation inductor: $L_c = 20$ μH; flying capacitor: $C_{ss} = 20$ μF; IGBT shunt capacitor: $C_s = 10$ nF; output filter inductor: $L = 40$ μH; output filter capacitor: $C = 1000$ μF, switching device: FF150R12RT4; and high-frequency rectifier diode: DPF240 × 200 NA. Figure 18 gives driving signals of four switching devices S_1, S_2, S_3, S_4 of the full-bridge three-level controlled-source circuit. S_1 and S_2 (or S_4 and S_3) are simultaneously turned on but with different turning off time. Output voltage and current are controlled by controlling pulse widths of S_1, S_4.

Figure 19 gives waveforms of secondary rectifying voltage u_d and commutation inductor current i_{L_c} of the high-frequency transformer. Commutation inductor current has different slopes under different output voltage values, but peak value point appears at converting the time of lagging leg, which solves difficult commutation problems of lagging leg and realizes soft switching of the controlled-source circuit within the whole power range.

Figures 20 and 21 give waveforms of primary u_{AB} and secondary rectifying voltage u_d as well as primary currents i_p of the high-frequency transformer in three-level DC/DC controlled-source circuit, respectively, under heavy load and light load. Under light load, switching devices also realize ZVS, which is identical to the theoretical analysis. Compared with two-level DC/DC controlled-source circuit, a level is added to secondary voltage, which results in a volume reduction of the output filter.

Figure 22 gives voltage waveforms at two ends of S_1 and S_2. Voltage borne by each switching device is half of the bus voltage, which greatly reduces voltage stress of switching device and solves large voltage stress problem of switching devices under high input voltage condition.

Figure 23 shows the output voltage and current waveforms of the three-level controlled-source circuit under step response. It can be seen from the figure that the output voltage ripple is small, and the dynamic response is fast.

Experimental prototype of marine electromagnetic transmitter is shown in Figure 24. The whole circuit is installed in a 23 cm (D) ∗ 780 cm (L) closed cylinder, with two ends connected with DC power supply and emitting electrode. Parameters include $V_{dc} = 540$ V, $V_o = 30$ V, $I_o = 200$ A, and $f_s = 20$ kHz. $L_c = 12$ μF, $L'_c = 20$ μF, $m = 20$, $n = 16$. Resonant inductor and commutation inductor are shown in Figure 25. Figure 26 gives change curves of three-level DC/DC controlled-source circuit efficiency with load change when resonant inductor and commutation reactor are used. Transmitter efficiency is improved, and maximum efficiency reaches 90% as the load increases. The main difference between the two lies in that when the load current is small, the transmitter using commutation inductor has higher efficiency.

6. Conclusions

For large voltage stress problem of switching devices in controlled-source circuit of marine electromagnetic detection transmitter under high input voltage condition, the three-level technology was used and voltage stress of switching device in the main circuit was reduced to half of the bus voltage, so this could reduce the rated voltage of

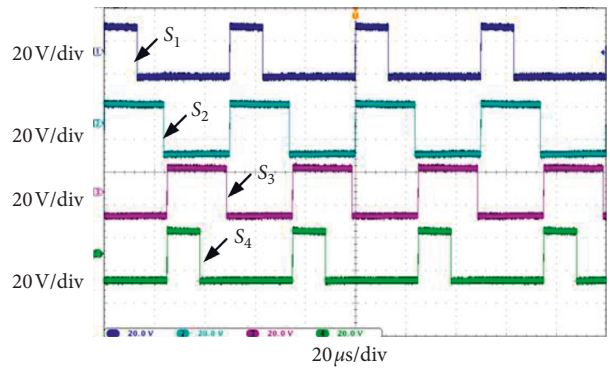

Figure 18: Driving waveforms of full-bridge three-level controlled-source circuit.

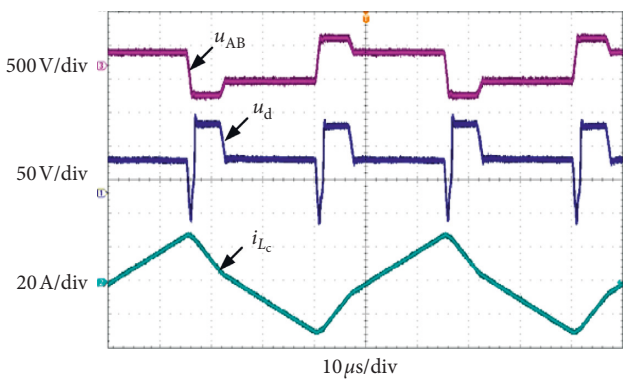

Figure 19: Waveforms of primary and secondary voltages of high-frequency transformer and commutation inductor current.

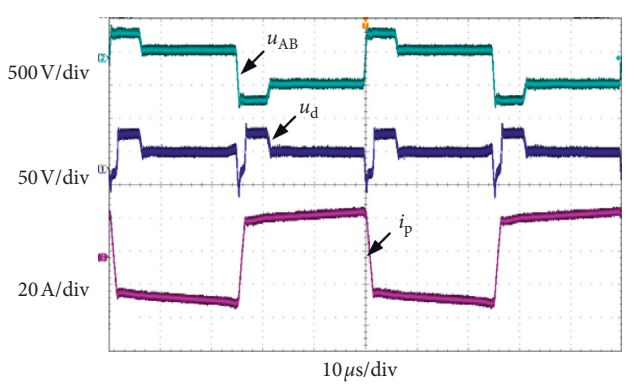

Figure 20: Waveforms of primary and secondary voltages and current of transformer under heavy load.

switching device, improve circuit operation efficiency, and reduce transformer and filter volumes.

In order to solve difficult current commutation problems of lagging legs, commutation inductor was added at the secondary side of the high-frequency transformer so as to realize soft switching of the controlled-source circuit within the whole power range and improve circuit efficiency. Moreover, this reduced requirement for leakage inductance of the high-frequency transformer and relieved transformer loss.

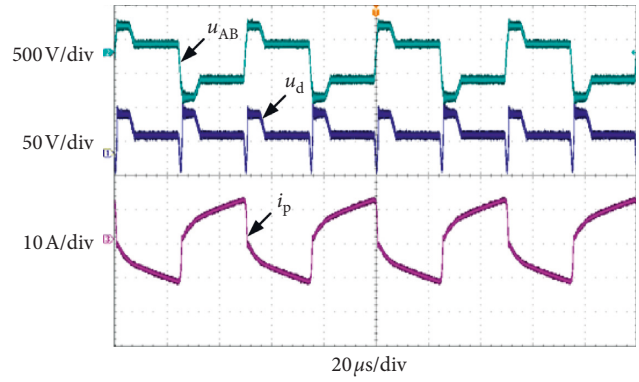

Figure 21: Waveforms of primary and secondary voltages and current of transformer under light load.

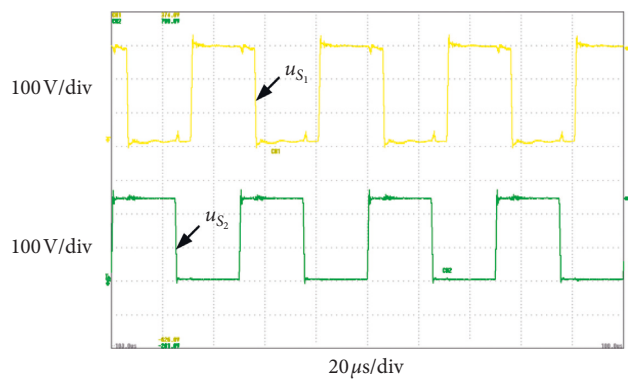

Figure 22: Voltage waveforms at two ends of S_1 and S_2.

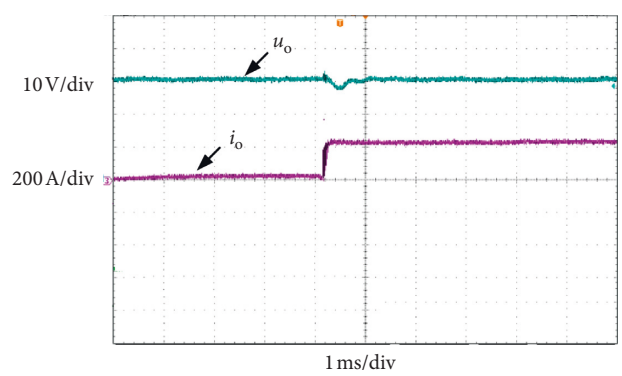

Figure 23: Circuit testing efficiency.

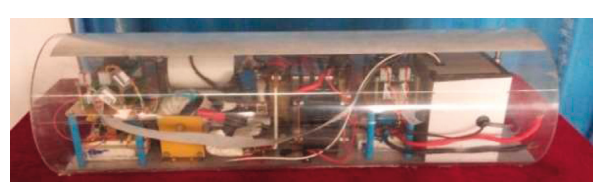

Figure 24: The physical picture of the marine transmitter.

On the condition that optimal control mode was satisfied, asymmetric phase-shift PWM control was introduced so that controlled duty ratio was corresponding to driving

(a) (b)

Figure 25: Resonant inductor and commutation inductor.

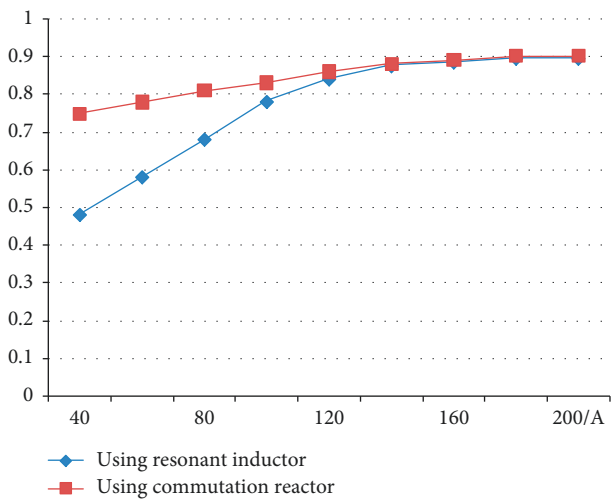

Figure 26: Circuit testing efficiency.

pulse width with definite physical significance, simple control, and convenience for the realization of digitalization.

Data Availability

The data used to support the findings of this study are available from the corresponding author upon request.

Conflicts of Interest

The authors confirm that this article content has no conflicts of interest.

Acknowledgments

The authors wish to acknowledge assistance or encouragement from colleagues, financial support by Henan mine power electronics device and control innovative technology team, Key research projects of Henan Higher Education Institutions (grant no. 18A410001), and Doctoral foundation of Henan Polytechnic University (grant no. B2017-19).

References

[1] M. Jegen, S. Holz, A. Swidinsky, and W. Bruckmann, "Quantification of marine sulfide deposits using marine electromagnetic methods," in *Proceedings of the Oceans'11 MTS/IEEE Kona*, pp. 1–8, Waikoloa, HI, USA, September 2011.

[2] N. Hussain, N. Karsiti, N. Yahya, and N. Yahya, "2D forward modeling of marine controlled source electromagnetic (CSEM) data for salt-dome and stratigraphy trap reservoir," in *Proceedings of the 4th International Conference on Intelligent and Advanced Systems (ICIAS2012)*, pp. 616–621, Kuala Lumpur, Malaysia, June 2012.

[3] K. Chen, W. Wen-bo, M. Dend et al., "Time synchronization for marine controlled source electromagnetic recorder," in *Proceedings of the 9th International Conference on Fuzzy Systems and Knowledge Discovery*, pp. 2519–2522, Chongqing, China, May 2012.

[4] G. Schultz, J. Miller, F. Shubitidze, and R. Evans, "Underwater controlled source electromagnetic sensing: locating and characterizing compact seabed targets," in *Proceedings of the of Oceans*, pp. 1–9, Hampton, VA, USA, October 2012.

[5] S. Constable and L. J. Srnka, "An introduction to marine controlled source electromagnetic methods for hydrocarbon exploration," *Geophysics*, vol. 72, no. 2, pp. WA3–WA12, 2007.

[6] H. Tao, Y. Zhang, and X. Ren, "Small-signal modeling of marine electromagnetic detection transmitter controlled-source circuit," *Mathematical Problems in Engineering*, vol. 2015, Article ID 754379, 9 pages, 2015.

[7] H. Tao, Y. Zhang, and X. Ren, "A novel circuit of marine controlled source electromagnetic transmitter," *Electric Power Components and Systems*, vol. 44, no. 9, pp. 1063–1070, 2016.

[8] Y. Zhang, C. Li, C. Zhu, C. Wang, and Z. Lan, "Three-level H-bridge cascade type multi-level inverter," *Transactions of China Electrotechnical Society*, vol. 26, no. 5, pp. 78–82, 2011.

[9] J. R Pinheiro and I. Barbi, "The three-level ZVS PWM converter-a new concept in high-voltage DC-to-DC conversion," in *Proceedings of the 1992 International Conference on Industrial Electronics, Control, Instrumentation, and Automation*, pp. 173–178, San Diego, CA, USA, November 1992.

[10] Z. Liu, X. Yu, and J. Ke, "A novel self-driven current-doubler-rectifier three-level converter with an integrated magnetic structure," *Transactions of China Electrotechnical Society*, vol. 30, no. 3, pp. 131–139, 2015.

[11] X. Zhang and C. Gong, "Three-level half-bridge voltage balancers," *Transactions of China Electrotechnical Society*, vol. 27, no. 8, pp. 114–119, 2012.

[12] T. Sun, T. Gao, H. Qu et al., "A ZVS three-level DC-DC converter with auxiliary transformer," *Proceeding of the CSEE*, vol. 31, no. 3, pp. 28–33, 2011.

[13] F. Liu, J. Yan, and X. Ruan, "Zero-voltage and zero-current-switching PWM combined three-level DC/DC converter," *IEEE Transactions on Industrial Electronics*, vol. 57, no. 5, pp. 1644–1654, 2010.

[14] Z. Zhang and X. Ruan, "Zero-voltage-switching PWM full-bridge three-level converter," *Proceeding of the CSEE*, vol. 25, no. 16, pp. 17–22, 2005.

[15] Y. Ma, X. Ruan, L. Zhou et al., "The best modulation strategy of the full-bridge three-level converter," *Proceeding of the CSEE*, vol. 23, no. 12, pp. 111–116, 2003.